International Journal of Thermal Sciences 48 (2009) 1932–1942

Contents lists available at ScienceDirect

International Journal of Thermal Sciences

journal homepage: www.elsevier.com/locate/ijts

Unsteady natural convection induced by diurnal temperature changes in a reservoir with slowly varying bottom topography

Tomasz P. Bednarz*, Chengwang Lei, John C. Patterson

School of Engineering, James Cook University, Townsville, QLD 4811, Australia

ARTICLE INFO

Article history:
Received 3 September 2008
Received in revised form
12 February 2009
Accepted 13 February 2009
Available online 21 March 2009

Keywords:
Natural convection
Reservoir
Exchange flow
Periodic thermal forcing
Topography

ABSTRACT

The present numerical investigation is concerned with the transient flow response in a reservoir model to periodic heating and cooling at the water surface. The numerical modelling reveals a stable stratification of the water body during the heating phase and an unsteady mixing flow in the reservoir during the cooling phase. It is shown that thermal instabilities play an important role in breaking up the residual circulation and initiating a reverse flow circulation in deep waters when the thermal conditions switch from heating to cooling. Further, if cooling is sufficiently strong, a clear undercurrent is formed, bringing cold water to the deep region of the reservoir. Moreover, heating from the water surface results in a stable large-scale convective roll which is clearly observed in the simulations. Understanding of the flow mechanisms pertinent to this problem is important for predicting the transport of nutrients and pollutants across reservoirs.

1. Introduction

Natural convection plays an important role in the transport of nutrients and pollutants between the near-shore and the central regions of lakes and reservoirs, and thus the understanding of the flow mechanisms pertinent to large-scale convective circulations in response to diurnal heating and cooling is very important from limnological points of view. In a typical diurnal cycle, the ambient temperature changes periodically, resulting in a varying thermal forcing acting on the water body. During nighttime cooling, near-shore horizontal temperature gradients are developed due to the fact that shallow regions cool relatively more quickly than deeper regions. The result is a cold water undercurrent proceeding along the bottom toward the deeper regions. At the same time, cooling at the water surface may generate plunging plumes from the surface. Conversely, during daytime heating, the input of solar radiation through the water surface results in relatively warm shallow regions. The absorption of solar radiation decreases with the water depth, resulting in a stable stratification in the water body. In shallow waters, the water depth is less than the penetration depth of solar radiation and thus some radiation reaches the bottom where the residual radiation is absorbed and the absorbed energy is re-emitted into the water layer above the bottom. This bottom heating is a destabilizing mechanism, which competes with the above-mentioned stable stratification. The bottom heating however, will not occur during a cloudy weather condition since there is no radiation. However, the vertical stable stratification may still be set up in the heating phase as a consequence of the temperature change at the water surface.

In the literature, several investigations of convective exchange flows in reservoirs have been reported. Horsch and Stefan [1] and Horsch et al. [2] investigated numerically and experimentally the convective circulation in littoral waters due to surface cooling in a triangular enclosure with a fixed heat flux at the surface. Their results illustrated transient development of the flow including the formation of sinking thermals and the establishment of a full cavity scale circulation. They have also examined the dependence of the flow development on different parameters of the model. Lei and Patterson [3] presented scaling analysis for the surface cooling case which revealed three laminar flow regimes, namely conductive, transitional and convective regimes, depending on the Rayleigh number. Their numerical simulations verified the scaling predictions. Recent experiments by Bednarz et al. [4] also confirmed the phenomena predicted in [3]. Earlier, Lei and Patterson [5–9] also studied the effect of daytime heating induced natural convection in a shallow wedge. They carried out experiments and corresponding two- and three-dimensional numerical simulations, and found that two-dimensional (2D) simulations were able to capture the major

* Corresponding author. Tel.: +61 7 4781 5218; fax: +61 7 4781 6788.
E-mail address: tomasz.bednarz@jcu.edu.au (T.P. Bednarz).

1290-0729/$ – see front matter © 2009 Elsevier Masson SAS. All rights reserved.
doi:10.1016/j.ijthermalsci.2009.02.011

Nomenclature

A	aspect ratio, $A = h/L$
g	acceleration due to gravity (m/s^2)
Gr	Grashof number, $Gr = g\beta\Delta T h^3/\nu^2$
h	maximum water depth (m)
h_x	local water depth (m)
L	length of the model (m)
n	coordinate normal to a surface (m)
p	period (s)
P	non-dimensional period
Pr	Prandtl number, $Pr = \nu/\alpha$
Q, $Q(x)$	averaged and local exchange flow rates
t	time (s)
T	temperature (K)
T_0	reference temperature (K)
u, v	velocity components in x and y directions (m/s)
U, V	non-dimensional velocity
x, y	coordinates in horizontal and vertical directions (m)

Greek symbols

α	thermal diffusivity (m^2/s)
β	coefficient of thermal expansion (1/K)
ν	kinematic viscosity (m^2/s)
ρ_0	density (kg/m^3)
θ	non-dimensional temperature
τ	non-dimensional time
ω	pressure (N/m^2)
Ω	non-dimensional pressure

features of the flow development, including the basic features of the flow instabilities and thus could be used to extract additional flow details with confidence. In a later study, Lei and Patterson [10] investigated flow responses to periodic heating and cooling in a reservoir model. In that study, the thermal forcing is by a periodic heat flux imposed at the water surface, which represents daytime solar radiation in the heating phase and nighttime heat loss in the cooling phase. The numerical results showed a time lag in the overall flow response when thermal forcing is switched between heating and cooling. This is consistent with the field observations of Adams and Wells [11] and Monismith et al. [12], and the analysis of Farrow and Patterson [13] and Farrow [14].

The present work extends, through numerical simulations, the previous investigations in a reservoir model with a periodic thermal forcing applied at the water surface. In this case, the periodic thermal forcing is by means of a varying surface temperature, corresponding to the effects of a varying ambient temperature but with no radiation input, as might be experienced during cloudy atmospheric conditions. This thermal forcing can be easily

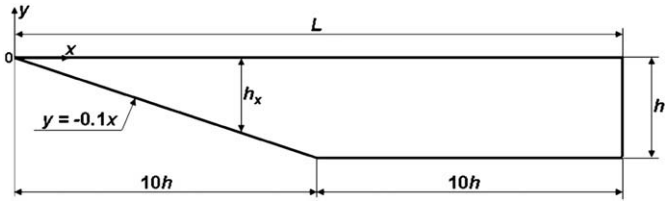

Fig. 1. Schematic of the considered reservoir model.

set up for small-scale laboratory experiments, which were investigated by the same authors [15].

2. Numerical model and procedures

2.1. Reservoir model

Fig. 1 shows a 2D reservoir model consisting of two distinct regions: one with a sloping bottom and the other with a uniform water depth. The total length of the model is L with a maximum water depth of h and a slope inclination of $A = 0.1$. A Cartesian coordinate system $(x - y)$ is adopted with the origin located at the tip of the reservoir model. As noted above, previous investigations showed that 2D numerical simulations can reproduce major flow features despite the three-dimensional (3D) nature of the instabilities under both heating and cooling conditions [3].

2.2. Governing equations and boundary conditions

The general form of the 2D governing equations for incompressible Newtonian fluid with the usual Boussinesq assumption is as follows:

$$\frac{\partial u}{\partial x} + \frac{\partial v}{\partial y} = 0, \tag{1}$$

$$\frac{\partial u}{\partial t} + u\frac{\partial u}{\partial x} + v\frac{\partial u}{\partial y} = -\frac{1}{\rho_0}\frac{\partial \omega}{\partial x} + \nu\left(\frac{\partial^2 u}{\partial x^2} + \frac{\partial^2 u}{\partial y^2}\right), \tag{2}$$

$$\frac{\partial v}{\partial t} + u\frac{\partial v}{\partial x} + v\frac{\partial v}{\partial y} = -\frac{1}{\rho_0}\frac{\partial \omega}{\partial y} + \nu\left(\frac{\partial^2 v}{\partial x^2} + \frac{\partial^2 v}{\partial y^2}\right) + g\beta(T - T_0), \tag{3}$$

$$\frac{\partial T}{\partial t} + u\frac{\partial T}{\partial x} + v\frac{\partial T}{\partial y} = \alpha\left(\frac{\partial^2 T}{\partial x^2} + \frac{\partial^2 T}{\partial y^2}\right), \tag{4}$$

where u and v are the velocity components in the x and y directions respectively, t is the time, ω is the pressure excluding hydrostatic pressure, T is the temperature, ρ_0 is the density at the reference temperature T_0, ν is the kinematic viscosity, g is the gravitational acceleration, β is the thermal expansion coefficient and α is the thermal diffusivity.

The initial and boundary conditions for the reservoir model presented in Fig. 1 are defined below.

Initially ($t \le 0$), the fluid is at rest and isothermal, that is

$$u = v = 0, \tag{5}$$

$$T = T_0. \tag{6}$$

The water surface ($y = 0$) is assumed to be stress-free, therefore

$$\frac{\partial u}{\partial y} = 0, \quad v = 0. \tag{7}$$

In order to simulate the diurnal cycles in field situations the temperature at the water surface varies from daytime to nighttime as follows:

$$T(t) = T_0 + \frac{\Delta T}{2}\sin\left(\frac{2\pi t}{p}\right), \tag{8}$$

where ΔT is the maximum temperature variation over a diurnal cycle and p is the period of diurnal cycles. This thermal forcing is illustrated in Fig. 2. During the first half of each cycle, the

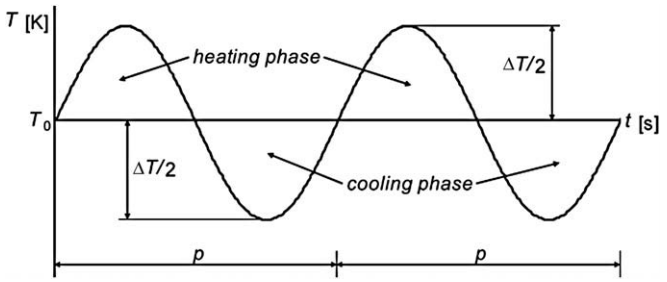

Fig. 2. Illustration of the transient temperature changes at the water surface.

temperature at the water surface is above the reference temperature T_0 and the system is in the heating phase, whereas during the second half of each cycle the system is in the cooling phase with $T < T_0$.

All other walls are assumed to be rigid, non-slip and adiabatic:

$$u = v = 0, \tag{9}$$

$$\frac{\partial T}{\partial n} = 0, \tag{10}$$

where n is the direction normal to the wall.

2.3. Non-dimensionalisation

The non-dimensionalisation of the governing equations is carried out by the method of Hellmus and Churchill [16].

Defining the dimensionless variables:

$$X = \frac{x}{x_0}, \quad Y = \frac{y}{y_0}, \quad U = \frac{u}{u_0}, \quad V = \frac{v}{v_0}, \quad \tau = \frac{t}{t_0},$$
$$\Omega = \frac{\omega}{\omega_0}, \quad \theta = \frac{T - T_0}{\Delta T},$$

and using the following scales:

$$\text{Length}(x, y): \; x_0 = y_0 = h$$

$$\text{Velocity}(u, v): \; u_0 = v_0 = \frac{\alpha}{h}$$

$$\text{Time}(t): \; t_0 = \frac{h}{u_0} = \frac{h^2}{\alpha}$$

$$\text{Pressure}(\omega): \; \omega_0 = \rho_0 u_0^2 = \rho_0 \frac{\alpha^2}{h^2}$$

$$\text{Temperature variation}(T - T_0): \; \Delta T$$

the governing equations can be rewritten as:

$$\frac{\partial U}{\partial X} + \frac{\partial V}{\partial Y} = 0, \tag{11}$$

$$\frac{\partial U}{\partial \tau} + U\frac{\partial U}{\partial X} + V\frac{\partial U}{\partial Y} = -\frac{\partial \Omega}{\partial X} + Pr\left(\frac{\partial^2 U}{\partial X^2} + \frac{\partial^2 U}{\partial Y^2}\right), \tag{12}$$

$$\frac{\partial V}{\partial \tau} + U\frac{\partial V}{\partial X} + V\frac{\partial V}{\partial Y} = -\frac{\partial \Omega}{\partial Y} + Pr\left(\frac{\partial^2 V}{\partial X^2} + \frac{\partial^2 V}{\partial Y^2}\right) + GrPr^2\theta, \tag{13}$$

$$\frac{\partial \theta}{\partial \tau} + U\frac{\partial \theta}{\partial X} + V\frac{\partial \theta}{\partial Y} = \frac{\partial^2 \theta}{\partial X^2} + \frac{\partial^2 \theta}{\partial Y^2}, \tag{14}$$

where Pr is the Prandtl number and Gr is the Grashof number. These two non-dimensional parameters characterise the important properties of the fluid and the thermal forcing.

The Prandtl number describes the relative strength of the diffusion of momentum to that of heat and is defined as:

$$Pr = \frac{\nu}{\alpha}. \tag{15}$$

The Grashof number expresses the ratio of buoyancy forces to viscous forces and is defined as:

$$Gr = \frac{g\beta\Delta T h^3}{\nu^2}. \tag{16}$$

The initial and boundary conditions are also rewritten in non-dimensional form as follows:

Initially, for $\tau \le 0$:

$$U = V = 0, \tag{17}$$

$$\theta = 0. \tag{18}$$

At the water surface:

$$\frac{\partial U}{\partial Y} = 0, \quad V = 0. \tag{19}$$

$$\theta(\tau) = 0.5 \sin\left(\frac{2\pi\tau}{P}\right). \tag{20}$$

On all other walls (including the deep end wall at $X = 20$), an adiabatic and rigid non-slip boundary condition applies, i.e.:

$$\frac{\partial \theta}{\partial n} = 0. \tag{21}$$

$$U = V = 0, \tag{22}$$

The influence of end wall on the flow development in the present configuration is confined to a region near the wall where the flow is turned around. Since the flow domain considered here is extended horizontally to include a region with a uniform water depth, the character of the flow above the slope, which is the major focus of this investigation, is unaffected by the end wall. Further discussion about the end-wall effects can be found in [3,14].

It is clear that during the cooling cycle there is the potential for instabilities to form as the surface cools to temperatures below the ambient. In principle, a linear stability analysis could be carried out to predict the criteria for the onset of the instabilities and their characteristics. However such an analysis requires knowledge of the base flow prior to instability, which in this case is unavailable. Further the time varying surface boundary condition would further complicate that analysis. It is much more straightforward to allow the numerical scheme to describe the instabilities.

2.4. Numerical scheme

In the present investigation the non-dimensionalised governing equations are numerically solved using a finite volume method [17,18] with a double precision solver. A second-order time-accurate formulation is employed in all calculations. Spatial derivatives are approximated using a third-order MUSCL scheme [19] which was conceived by blending a central differencing scheme and a second-order upwind scheme. Pressure–velocity coupling is carried out using the SIMPLE algorithm [17]. The absolute convergence criteria for the numerical solutions are specified based on the

residual sums of all conserved quantities. If the residual sum is less than 10^{-5} for each conserved quantity, the equations are deemed to have converged at a specific time.

2.5. Numerical parameters

The present investigation is pertinent to the modelling of unsteady convective exchange flows in reservoirs or lakes with water as the working fluid. Therefore the Prandtl number is fixed at $Pr = 7.07$ (at the reference temperature $T_0 = 20\,^{\circ}C$). The numerical simulations are based on a laboratory scaled reservoir model with a full length of 0.3 m, a maximum water depth of 0.015 m and a bottom slope of 0.1 in the sloping region [4]. Scaling of the physical system to an achievable laboratory model using water as the model fluid is not feasible. Consequently, the physical size of both the experiment and the numerical simulation is determined by the ability to demonstrate the physical mechanisms which occur, rather than as a means of predicting actual flows in the physical system. A minimum period of 14 min can be achieved in our lab for cycling the water surface temperature [20]. Accordingly, based on the laboratory model and a room temperature of 20 °C, the dimensionless period of the thermal forcing is set to $P = 0.53$ in the present simulation. The purpose of this numerical simulation is to show the flow mechanisms that are relevant to real physical systems with a very small temperature changes over the diurnal cycle.

The present numerical simulations are conducted for Grashof numbers over the range of 10^3–10^7. A non-uniform grid system (with a maximum grid stretching factor of 1.05) is constructed with finer grids distributed in the vicinity of all the wall boundaries, close to the tip region and where the slope finishes. Three different meshes (431×26, 861×51 and 1281×76) were tested to check the dependence of the numerical solutions on the grid resolution. The averaged volumetric flow rate Q defined later in Eq. (24) is chosen for comparison purposes. The mesh dependence test is carried out for the most unstable case with $Gr = 10^7$ and $Pr = 7.07$, and the result is shown in Fig. 3. This is a maximum actual value of Gr achieved in a cycle, and related numerical studies [21] have shown that at this value of Gr for cooling, the flow remains laminar. At very high Gr, the flow may become turbulent and a turbulence model would be required. That case is not considered here.

It is seen in Fig. 3 that in the thermal cycles depicted all the three solutions with different meshes are generally consistent except in the most unstable stage of the flow development when instabilities in the form of randomly distributed sinking plumes occur (refer to Section 3 for further information). Since the present investigation aims to characterise the overall flow development over diurnal cycles rather than resolving details of the flow instabilities, which are very sensitive to the grid resolution, the medium mesh 861×51 is adopted in all subsequent computations in consideration of both the numerical accuracy and the computing time. A time-step dependence test has also been carried out for the largest Grashof number case and an optimal dimensionless time-step is chosen to be 5.3×10^{-5} for the present study, resulting in a maximum "Courant–Friedrichs–Lewes" (CFL) number of 1.472 for $Gr = 10^7$. The CFL number provides an indication of numerical stability and accuracy. In general a smaller CFL number would produce more accurate numerical results than a larger CFL number. A CFL number less than unity is required for explicit numerical schemes to ensure stability of the numerical solutions. However, this is not necessary for implicit numerical schemes such as the one used in the present investigation. More discussion of the CFL number effect can be found in [22].

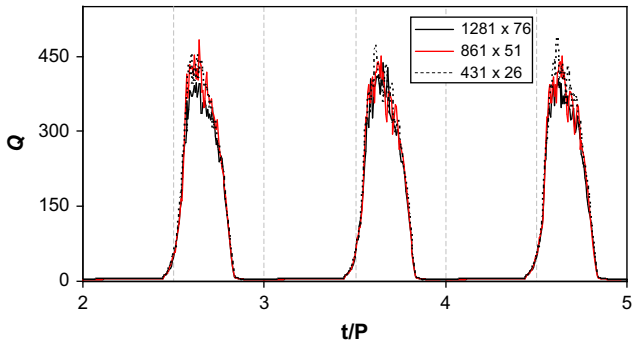

Fig. 3. Time histories of the calculated horizontal exchange flow rates for $Pr = 7.07$ and $Gr = 10^7$ with three different meshes for thermal cycles 3–5.

3. Results

Figs. 4–6 plot the isotherms (left column) and corresponding streamlines (right column) at representative times over a typical diurnal cycle for three different Grashof numbers ($Gr = 10^3$, 10^5, and 10^7, respectively). The times indicated on these figures start at the beginning of the tenth cycle ($t/P = 9.0$) after the flow has reached a quasi-steady state. The values on the isotherms represent the numerical values of the temperature, and in the streamline plots, solid lines indicate a clockwise circulation, and dashed lines indicate a counter-clockwise circulation.

3.1. Flow response to periodic temperature changes at $\mathrm{Gr} = 10^3$

At $t/P = 9.0$, i.e., at the beginning of the tenth cycle, the thermal condition at the water surface switches from cooling to heating. However, the residual temperature and flow structures formed in the previous cooling phase can be still observed in Fig. 4(a). In particular, the presence of convective cells from the cooling phase is still evident in the main body of the domain. Underneath the top water surface, a distinct boundary layer of relatively warmer fluid is created by conduction. At this particular moment, i.e., when $t/P = 9.0$, the system switches from cooling to heating, however the temperature at the water surface actually starts to increase one quarter cycle earlier. As a consequence, the cooling effect is being weakened in the second half of the cooling phase and a relatively warmer fluid layer is forming underneath the water surface, pushing the relatively colder fluid toward the bottom. In the shallow region (close to the tip), the isotherms curl over in order to satisfy the zero heat flux condition on the sloping bottom which requires that the isotherms become perpendicular to the slope. As a consequence, a negative horizontal temperature gradient is established, which is responsible for the generation of a convective flow in the clockwise direction in the tip region, seen from the streamlines in Fig. 4(a). At this stage of the flow development, the whole computational domain has a cellular flow pattern.

As the heating proceeds, the upper region of the flow domain becomes stably stratified, as seen in Fig. 4(b). The clockwise circulation roll from the tip region expands toward the deep region and some of the convective cells in the main body merge together to form larger cells. However, the flow itself becomes weaker due to the stabilizing effect of heating from the water surface. At $t/P = 9.50$ (Fig. 4(c)), the heating switches to cooling and the situation reverses. Prior to this time, the surface temperature has been decreasing, and a boundary layer of relatively colder fluid has formed underneath the water surface. Due to the same mechanism as described above, which requires isotherms to be perpendicular to the sloping bottom, a positive temperature gradient is established in the tip region, creating a counter-clockwise circulation there. The previously formed clockwise convective roll above the sloping bottom shifts toward the central region, and a large but weak counter-clockwise convective roll is observed in the deeper

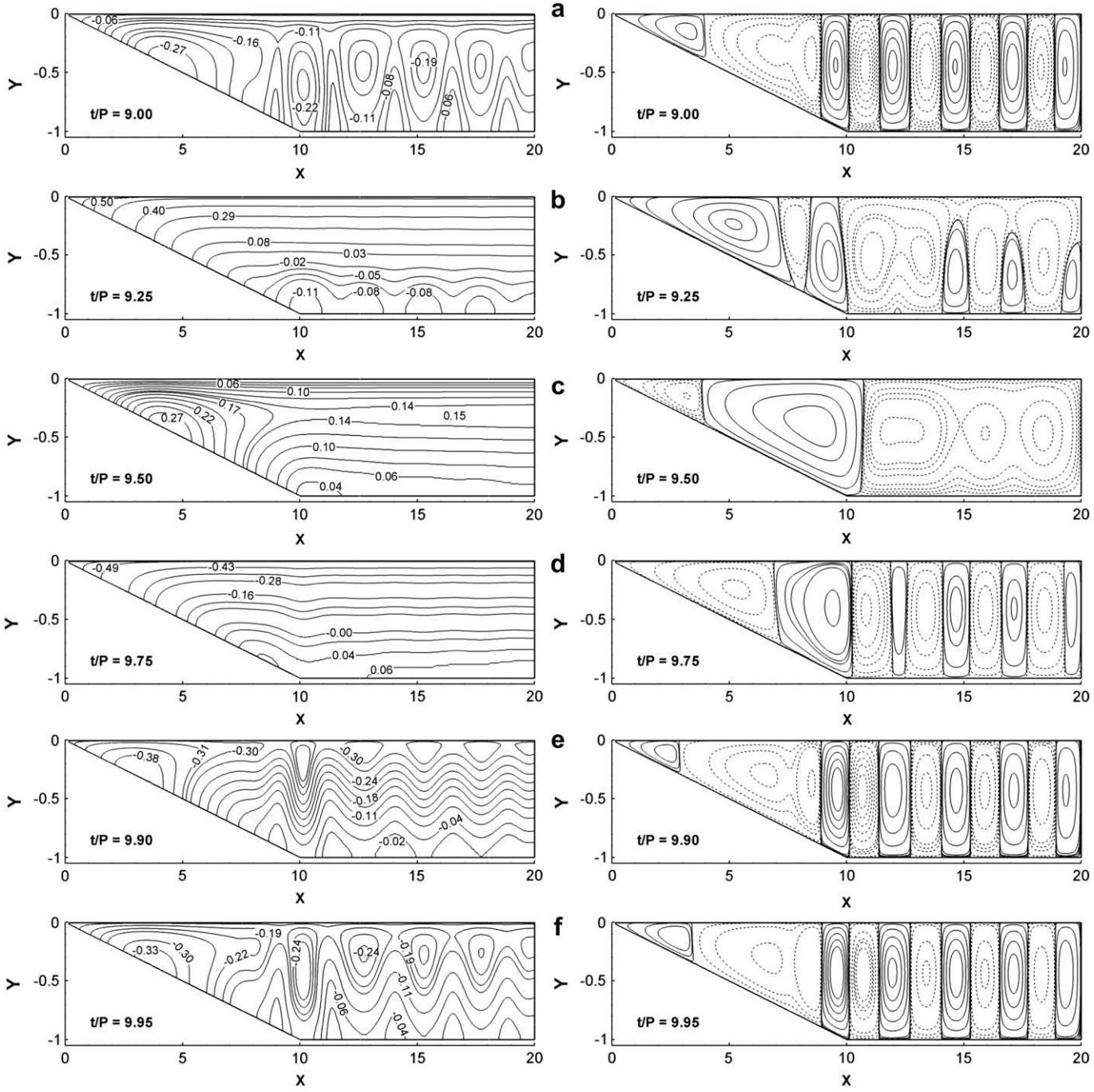

Fig. 4. Different stages of the flow response to diurnal thermal forcing in shallow waters of a reservoir at $Gr = 10^3$. Left: isotherms, right: streamlines.

region. As the cooling proceeds, at $t/P = 9.75$, when the surface temperature is at its minimum value, weak instabilities due to the destabilizing effect of cooling from above can be observed in the isotherms (Fig. 4(d)) and corresponding convective cells are seen from the streamlines. Flow instabilities are also evident in the second half of the cooling phase, as shown in Fig. 4(e–f). A similar cellular flow structure is observed at times $t/P = 9.90$ and 9.95. However, during the second half of the cooling phase, the fluid near the surface is slowly heating up, and an expanding clockwise roll is forming in the tip region due to the negative horizontal temperature gradient there.

The flow development throughout the whole thermal cycle at $Gr = 10^3$ results in an always present, but ever changing, cellular flow pattern in the computational domain, indicating that the convective circulations are always present, even with the weak thermal forcing. The results suggest that even in such a weak thermal flow, mixing accompanies the diurnal cycle. The next sections describe the flow evolutions at higher Grashof numbers of $Gr = 10^5$ and 10^7.

3.2. Flow response to periodic temperature changes at $\mathrm{Gr} = 10^5$

At the beginning of the cycle (at $t/P = 9.0$), the surface cooling switches to surface heating. The residual temperature and flow structures formed in the previous cooling phase are still present. The isotherms presented in Fig. 5(a) clearly show that a layer of

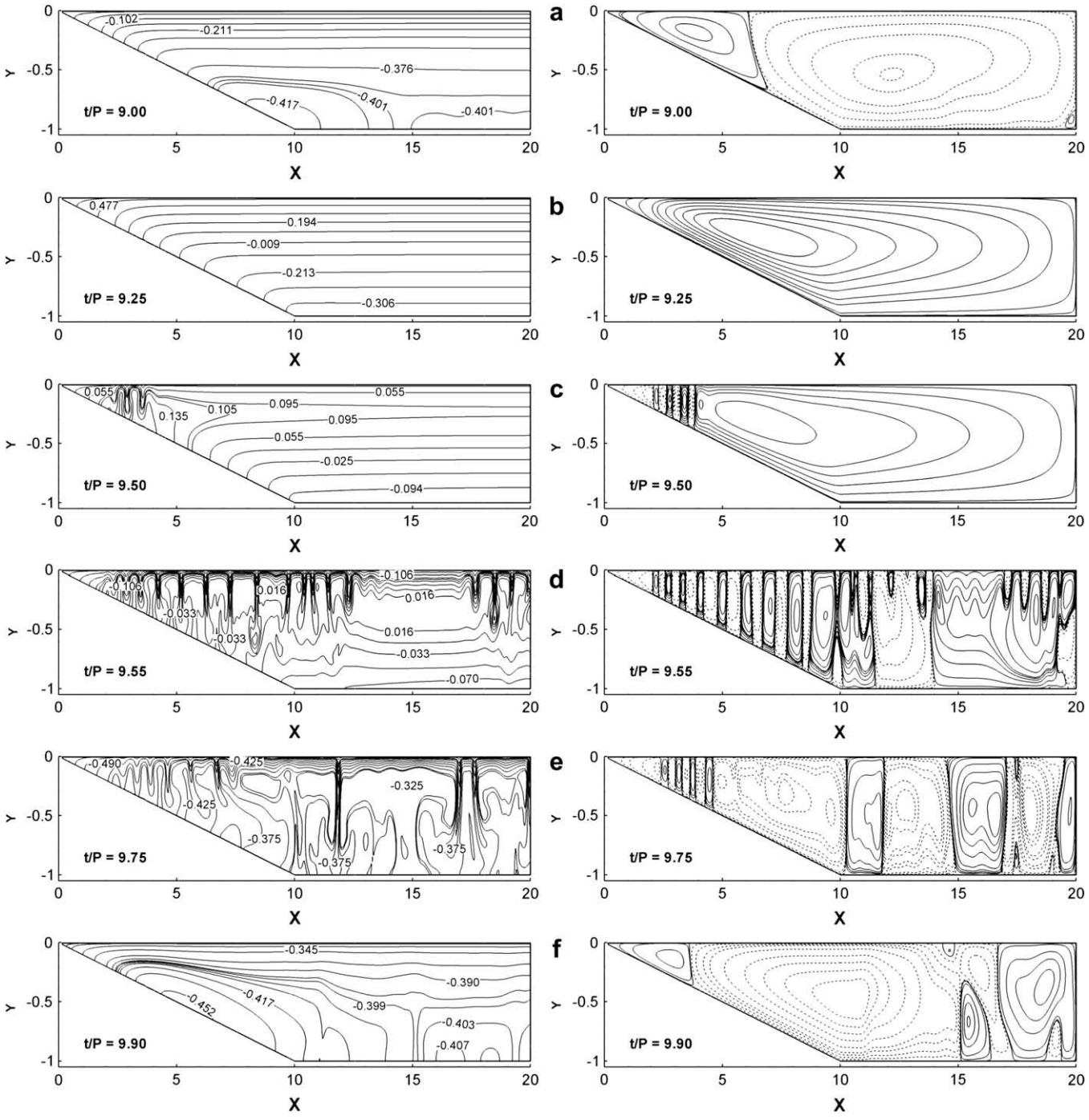

Fig. 5. Different stages of the flow response to diurnal thermal forcing in shallow waters of a reservoir at $Gr = 10^5$. Left: isotherms, right: streamlines.

relatively warmer fluid formed beneath the water surface as the surface temperature increases from its minimum value. A residual anticlockwise circulation arising from the previous cooling phase remains in the central part of the domain. The tip region heats up more quickly and a negative horizontal temperature gradient is created. As a consequence, a clockwise circulation forms in the tip region, as in the previous case, and a downwelling region is formed. The tip driven clockwise circulation expands toward the deep region as heating proceeds and, unlike the previous case, eventually encompasses the entire domain, as seen in Fig. 5(b). Thus, in general, the heating from the water surface works to stabilise and reverse the convective motion that is carried over from the previous cooling stage.

At $t/P = 9.25$ (maximum of the heating), as seen in Fig. 5(b), the temperature profiles are already stably stratified and as mentioned above, a full domain clockwise circulation is present. This stable stratification and full domain circulation will be broken when the top water surface is cooled at a sufficient rate. At $t/P = 9.50$, the heating switches to cooling, and clear convective instabilities are already observed in the tip region as seen in Fig. 5(c) as the surface is actually cooler than the water temperature underneath the surface despite that the thermal forcing is still in the heating

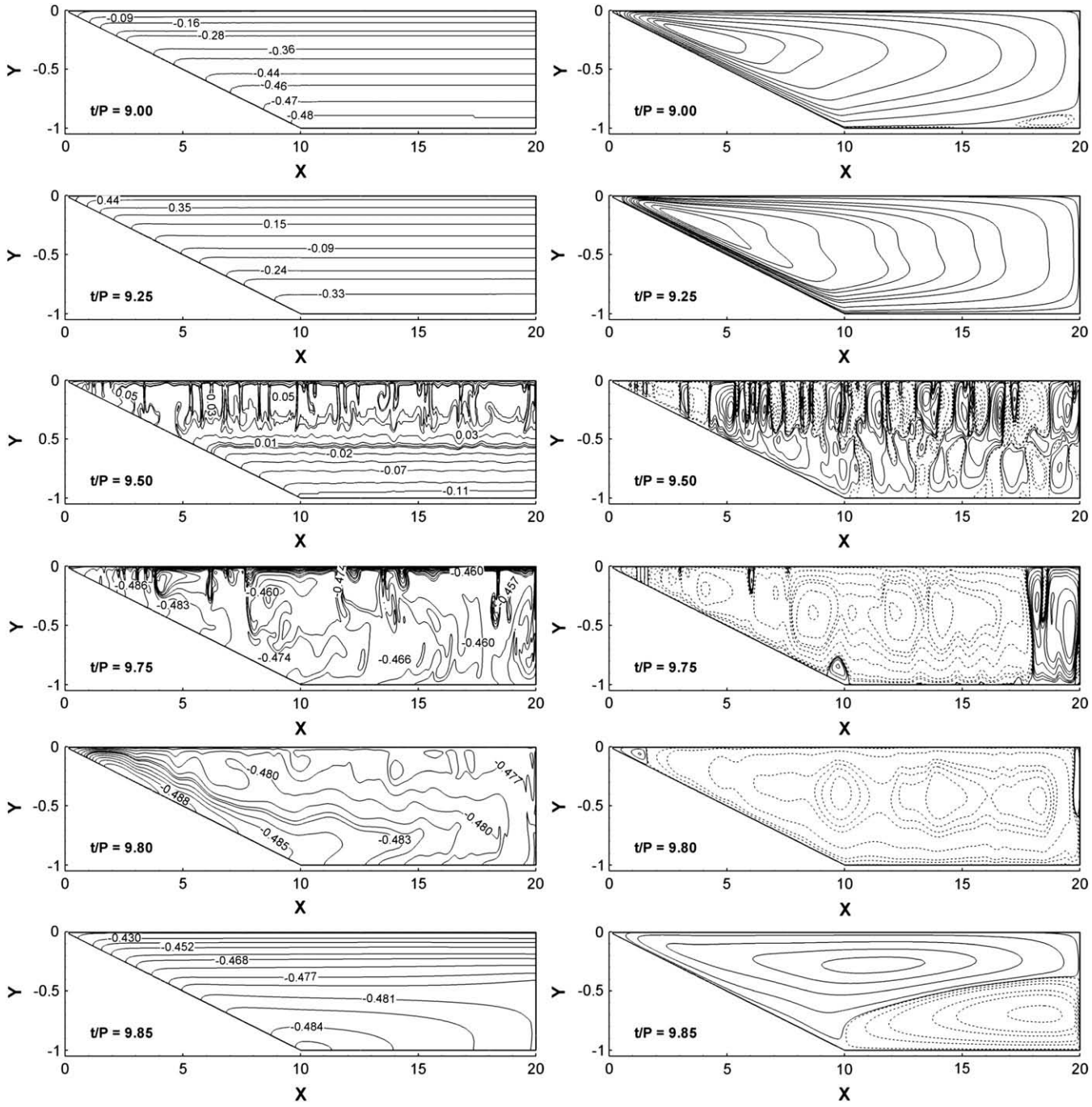

Fig. 6. Different stages of the flow response to diurnal thermal forcing in shallow waters of a reservoir at $Gr = 10^7$. Left: isotherms, right: streamlines.

phase before this time. Since the cooling is from the top, the fluid immediately below the surface becomes denser and heavier relative to the interior region and because the tip region cools more quickly, the instabilities always start from there after a certain critical condition is met. At this stage, the plumes are relatively week and are just starting to penetrate the local water depth. They will intensify as the cooling at the water surface continues. In the region above the slope (close to the tip), where the instabilities occur, intensive mixing is observed from the streamlines in Fig. 5(c). In the deep water region, the clockwise convective roll that is developed earlier in the heating phase still dominates the flow.

At $t/P = 9.55$, cold water thermals are clearly present along the whole top surface as seen in Fig. 5(d). These plumes penetrate the local water depth in the form of Rayleigh–Benard convection, carrying colder surface water to the bottom, where they are prone to overturning and mixing with the ambient fluid. Close to the tip, where the water cools more quickly, a positive horizontal temperature gradient is created which carries cold water down the slope toward the deeper water region and results in an undercurrent in the later stage of the flow. Therefore, at $t/P = 9.55$, a counter-clockwise circulation in the tip region is observed. The streamlines at this stage of the flow also suggest that the convective circulations occur in the whole water body and enhance the local mixing.

At $t/P = 9.75$, the water surface temperature reaches its minimum. Distinct plunging thermals can be still observed and also a cold but weak and not yet fully developed undercurrent proceeding down the bottom slope can be seen in Fig. 5(e). At this time, the undercurrent has reached the end of the sloping region. It is possible to observe three distinct regions of the flow in Fig. 5(e): the undercurrent on the sloping bottom, a surface return flow which moves under the water surface toward the shallow end, and the deep region dominated by large sinking plumes. The return flow, unlike the undercurrent, is very unstable as the surface is still being cooled. Sinking plumes burst intermittently from the return flow below the water surface and break the large counter-clockwise circulation in the region close to the tip, as seen in Fig. 5(e).

At $t/P = 9.90$, the top water surface temperature is increasing, but the overall system is still in the cooling phase. The top water surface is stabilized by a relatively warmer fluid layer and there are no plunging thermals observed at this stage. It is also noticeable that the previously formed cellular flow pattern is slowly being replaced by a large evolving counter-clockwise convective circulation in the core part of the enclosure. Close to the tip, a clockwise circulation is forming as the tip region heats up at a higher rate. The residual temperature and flow structures formed in the previous stages are still present in the lower part of the reservoir model as seen in Fig. 5(f).

3.3. Flow response to periodic temperature changes at $\mathrm{Gr} = 10^7$

At $Gr = 10^7$, the general flow characteristics are similar to the previous case and may be described in a similar way. Therefore, for brevity, the detailed description is not included here. The major difference is that due to the increased strength of thermal forcing, the flow response is faster. For instance, the full enclosure clockwise circulation can be already observed at $t/P = 9.00$ (see Fig. 6(a)), i.e., when the forcing switches from cooling to heating, and a stable stratification of the temperature is already achieved at the start of the cooling phase. Also, thermal instability in the form of plunging plumes occurs at a higher rate (compare Fig. 5(c) with Fig. 6(c)). The most distinct feature at $Gr = 10^7$ is that a domain-wide counter-clockwise convective roll is generated in the cooling phase, as seen from the streamlines in Fig. 6(e). From the corresponding isotherms in Fig. 6(e), a distinct domain-wide undercurrent is observed. This is not observed for the lower Grashof number cases, in which the cooling rate is not sufficiently high for the undercurrent to develop over the full length of the reservoir model.

3.4. Temperature histories over a full thermal cycle

Fig. 7 shows the time series of the minimum, maximum and volume averaged temperatures recorded over one full thermal cycle for $Gr = 10^3, 10^5$ and 10^7 along with the specified temperature at the water surface (all temperatures are in the non-dimensional form and are obtained by solving the dimensionless governing equations (11–14) with the normalized temperature (20) applied at the water surface). In these plots, several dynamic temperature behaviours can be observed. First, for all the Gr values the plots of the maximum temperature value in the computational domain coincide with the plots of the applied surface temperature in the first half of the heating phase. From the previous sections, it is known that the flow structures are being stabilized as they are in the heating phase. This happens because the heating occurs from above and conduction plays a significant role in establishing a stable stratification of the temperature below the water surface. Until $t/P = 9.25$ the water surface temperature gradually increases and so does the maximum temperature due to the conduction effect.

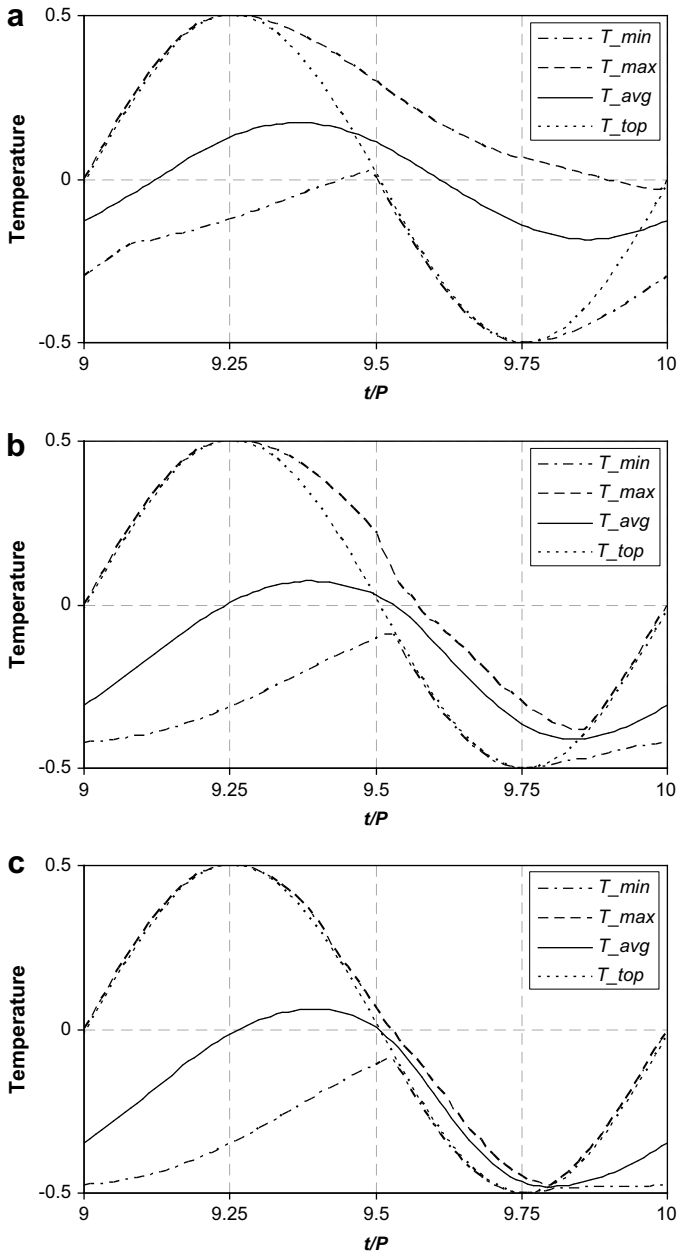

Fig. 7. Minimum, maximum, average and surface temperature histories over one full thermal cycle at (a) 10^3, (b) 10^5 and (c) 10^7.

After $t/P = 9.25$, the surface temperature starts to drop. Beneath the water surface a new thermal boundary layer of relatively colder fluid develops. The rate of the development of this thermal layer depends on the cooling rate which is characterised by the Grashof number. For the smallest Grashof number case, the dynamic response of the system is slow as the conduction effect plays an important role in the flow response, and relatively warmer fluid regions are present for a longer period (Fig. 7(a)). On the other hand, for the larger Grashof number cases, the thermal layer of colder fluid grows more quickly; after a relatively shorter time a critical condition is met; and thermal instabilities occur, carrying relatively colder surface water toward the bottom and mix the water over local water depths (Fig. 7(b and c)). It can be seen that the maximum temperature in the computational domain decreases more abruptly when the cooling rate is stronger as the thermal instabilities cause enhancement of mixing of the fluid body.

When the surface temperature increases (after $t/P = 9.75$), the maximum fluid temperature in the computational domain continues to decrease until the time when the maximum temperature matches the surface temperature. This cooling effect until that moment is obvious, as the surface temperature, even in an increasing trend is still less than the maximum temperature monitored in the enclosure. Also from that moment the creation of a stabilizing surface boundary layer of relatively warmer fluid becomes evident. From Fig. 7(a–c), it can be seen that the higher the Grashof number, the earlier the heating effect appears in the system, i.e., the earlier the descending maximum temperature plot meets the surface temperature plot.

Further, the minimum temperature of the fluid in the computational domain, as seen from Fig. 7(a–c), always increases in the heating phase (from $t/P = 9.0$ to $t/P = 9.5$) until it matches the water surface temperature. The minimum temperature then follows the surface temperature over the first half of the cooling phase. This is explained by the conduction flow regime being created close to the tip region which controls the minimum temperature (the cooling of the water body always occurs more quickly close to the tip region). When the water surface temperature starts to increase (after $t/P = 9.75$), the minimum temperature in the water body also starts to increase. The higher the Grashof number the slower the increase as the result of the amount of relatively colder fluid that remained close to the bottom from the earlier flow stages. This is the result of relatively cold fluid carried in to the bottom by the undercurrent. At higher Grashof numbers, this fluid remains in the region above the bottom for longer periods.

The time histories of the spatially averaged temperature over the entire computational domain, marked with the solid lines in Fig. 7(a–c), show that the occurrence of the maxima and minima of the spatially averaged temperature is always out of phase with the thermal forcing over the cycle. Further, it can be noticed in Fig. 7(a), that for the smallest Grashof number ($Gr = 10^3$) case, in which conduction plays an important role in the flow development, the spatially averaged temperature cycles about a zero mean value, indicating that the total heat input to the water body during the heating phase is about the same as the total heat loss from the water body during the cooling phase. However, this situation is different for the higher Grashof number cases (Fig. 7(b and c)), in which the spatially averaged temperature cycles about a negative mean value, indicating that more heat is lost from the water body during the cooling phase than that gained by the water body during the heating phase. The imbalance between the heat gain and the loss over a diurnal cycle increases with the Grashof number. The above observation suggests that during cloudy conditions, the cooling effect would dominate the convective motion in reservoirs.

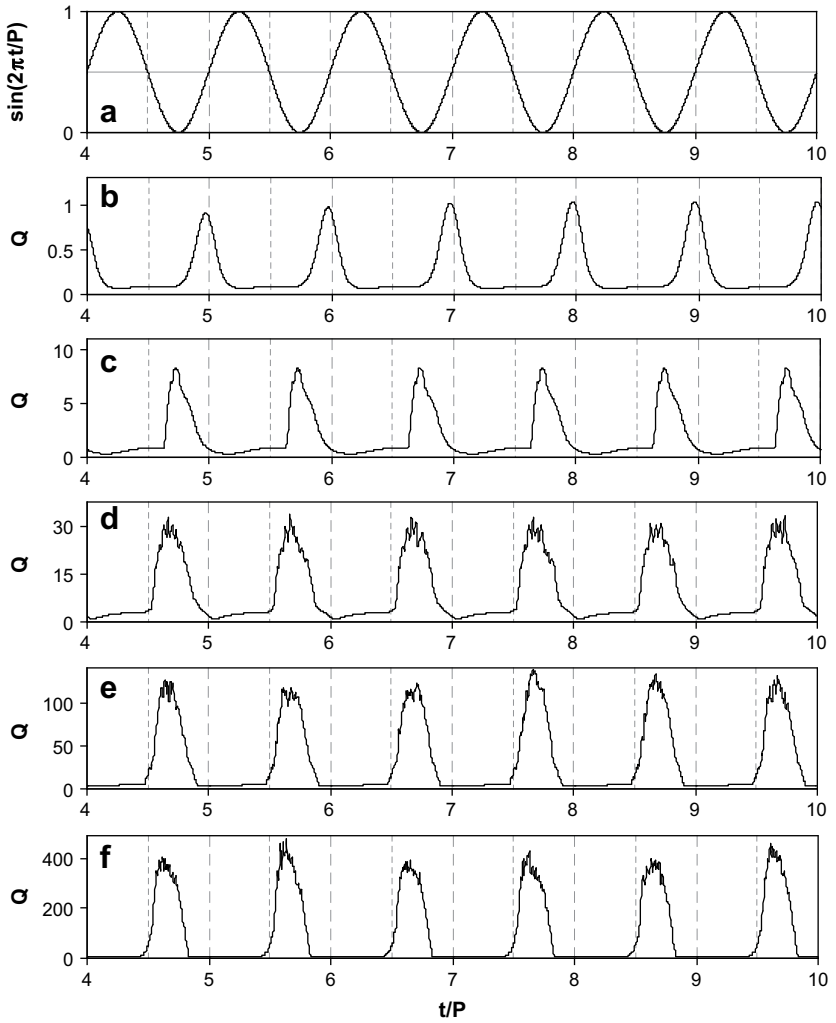

Fig. 8. Time histories of (a) the thermal forcing at the water surface; the calculated horizontal exchange flow rate at $Pr = 7.07$ and for different Grashof numbers (b) 10^3, (c) 10^4, (d) 10^5, (e) 10^6 and (f) 10^7.

3.5. Horizontal exchange flow rate

In order to explore additional features of the flow response to the periodic thermal forcing, an averaged horizontal volumetric flow rate Q is calculated [3,10]:

$$Q = \frac{1}{L}\int_0^L Q(x)\mathrm{d}x, \tag{23}$$

where L is the total length of the flow domain, and $Q(x)$ quantifies the intensity of the horizontal exchange flow at a given x location and is defined as follows:

$$Q(x) = \frac{1}{2}\int_{-h_x}^{0} |u|\mathrm{d}y. \tag{24}$$

Here, the dimensional exchange flow rate has been normalised using the scale $\sim\alpha$.

Fig. 8 shows the time histories of the calculated averaged horizontal exchange flow rates at $Pr = 7.07$ and for five different Grashof numbers ($Gr = 10^3$, 10^4, 10^5, 10^6 and 10^7) along with the imposed thermal forcing at the water surface. In these plots Q is plotted for six consecutive thermal cycles (cycles 5–10). The time periods in Fig. 8(a) over which $\sin(2\pi t/P) > 0$ represent the daytime heating phase whereas those over which $\sin(2\pi t/P) < 0$ represent the nighttime cooling phase. At $t/P = 4$, 5, 6, etc. the thermal forcing is switched from nighttime cooling to daytime heating.

In general, the time histories of the horizontal exchange flow rates for different Grashof numbers demonstrate certain common features. As seen in Fig. 8, the exchange flow rates exhibit a periodic behaviour in response to the periodic changes of the temperature at the water surface. Also, the flow response is clearly out of phase with the thermal forcing and in each cycle, time periods with both weak and intense flow responses are observed. The weak-response periods correspond to the flow response to daytime heating, which stabilizes the flow as described above. On the other hand, the intense-response periods clearly correspond to nighttime cooling, caused mostly by the presence of strong convective instabilities in the form of plunging thermals. Fig. 8 also shows that the intensity of the flow response increases with the Grashof number.

Consider first the case of a relatively small Grashof number ($Gr = 10^3$) shown in Fig. 8(b). It is seen in this figure that, in contrast to the increasing thermal forcing, the averaged horizontal flow rate decreases from $t/P = 4$ until $t/P = 4.25$. After $t/P = 4.25$, the averaged horizontal flow rate starts to increase, but the water surface temperature has already started to decrease. This observation indicates that the time lag of the flow response to the switch of the thermal forcing from cooling to heating is approximately one quarter of the thermal forcing period for the present Grashof number. On the other hand, during the cooling phase, the maximum response is obtained at $t/P = 4.965$, indicating also a time lag in switching from cooling to heating. Therefore, it can be concluded that for low Grashof numbers the response of the flow to the switch of the thermal forcing is very slow, as conduction may play an important role in the resulting flow.

At $Gr = 10^4$, the time history of the averaged horizontal exchange flow rate exhibits similar features. However, the first minimum and the maximum peak of the flow response are shifted toward left-hand side. The minimum occurs at $t/P = 4.145$, and it corresponds to the switch from nighttime cooling to daytime heating. The time lag of that switch is approximately 14.5% of the thermal forcing period. The peak corresponding to the cooling phase occurs at $t/P = 4.7$. The plot of the averaged horizontal flow rate is smooth as the convective motion is still relatively weak. However, it is observed that for larger Grashof numbers (e.g., $Gr = 10^5$) the nighttime cooling response has some irregularities caused by strong convective instabilities in the form of plunging thermals. The same is observed for $Gr = 10^6$ and 10^7. At these two Grashof numbers, the start of instabilities can be observed during the heating phase before heating switches to cooling.

4. Conclusions

In the present study, the quasi-steady natural convection flow in a reservoir model subject to periodic thermal forcing at the water surface is described, based on numerical results. The present numerical simulations have revealed the general characteristics of the flow development relevant to cloudy atmospheric conditions when solar radiation is not present in the system and the flow is driven solely by the ambient temperature changes. It is observed that the primary convective circulation in the reservoir changes its direction when the thermal forcing switches from cooling to heating and vice versa. It is also revealed that there is a time lag of the flow response to the switch of the thermal forcing from cooling to heating which depends on the strength of thermal forcing as characterised by the Grashof number. The calculated horizontal exchange flow rates based on the calculated velocity fields showed that the overall strength of the circulation in the heating phase is significantly weaker than that in the cooling phase, suggesting that during cloudy conditions, the cooling effect dominates the convective motion in reservoirs.

The unsteady flow structures and stable stratifications obtained in the present numerical simulations have also been observed in our recent experiments carried out in a reservoir model cooled and heated from above in diurnal cycles [15], in which the development of unsteady convection is described based on experimental flow visualization and quantitative temperature and velocity measurements with thermo-chromic liquid crystals. The experimental results confirm the general behaviour of the flow development as described in this paper.

The numerical results presented herein indicate also that the convective motions in reservoirs in diurnal cycles are very important from environmental and ecological points of view. Water circulation driven by horizontal thermal gradients may cause the transport of small suspended pollutants or biological particles or dissolved constituents into or from deep water regions and thus plays a significant role in determining water quality. The present paper however, considers only numerical results of convective motion in diurnal cycles. Further study of particle transport, which is beyond the scope of the present investigation, will help to understand how the relative phase and motions of particles may be calculated and applied to the ecological transport models. Also, the present numerical results will be compared with experimental results arising from the next stage of the project.

Acknowledgment

The authors gratefully acknowledge the financial support of the Australian Research Council (ARC).

References

[1] G.M. Horsch, H.G. Stefan, Convective circulation in littoral water due to surface cooling, Limnology and Oceanography 33 (5) (1988) 1068–1083.
[2] G.M. Horsch, H.G. Stefan, S. Gavali, Numerical simulation of cooling-induced convective currents on a littoral slope, International Journal for Numerical Methods in Fluids 19 (1994) 105–134.
[3] C. Lei, J.C. Patterson, Unsteady natural convection in a triangular enclosure induced by surface cooling, International Journal of Heat and Fluid Flow 26 (2005) 307–321.
[4] T. Bednarz, C. Lei, J.C. Patterson, An experimental study of unsteady natural convection in a reservoir model cooled from the water surface, Experimental Thermal and Fluid Science 32 (2008) 844–856.

[5] C. Lei, J.C. Patterson, Unsteady natural convection in a triangular enclosure induced by absorption of radiation, Journal of Fluid Mechanics 460 (2002) 181–209.
[6] C. Lei, J.C. Patterson, Natural convection in a reservoir sidearm subject to solar radiation: experimental observations, Experiments in Fluids 32 (2002) 590–599.
[7] C. Lei, J.C. Patterson, A direct stability analysis of a radiation-induced natural convection boundary layer in a shallow wedge, Journal of Fluid Mechanics 480 (2003) 161–184.
[8] C. Lei, J.C. Patterson, A direct three-dimensional simulation of radiation-induced natural convection in a shallow wedge, International Journal of Heat and Mass Transfer 46 (7) (2003) 1183–1197.
[9] C. Lei, J.C. Patterson, Natural convection in a reservoir sidearm subject to solar radiation: a two-dimensional simulation, Numerical Heat Transfer, Part A: Applications 42 (1) (2002) 13–32.
[10] C. Lei, J.C. Patterson, Natural convection induced by diurnal heating and cooling in a reservoir with slowly varying topography, JSME International Journal, Series B: Fluids and Thermal Engineering 49 (3) (2006) 605–615.
[11] E.E. Adams, S.A. Wells, Field measurements on side arms of Lake Anna, Va, Journal of Hydraulic Engineering 110 (1984) 773–793.
[12] S.G. Monismith, J. Imberger, M.L. Morison, Convective motions in the sidearm of a small reservoir, Limnology and Oceanography 35 (1990) 1676–1702.
[13] D.E. Farrow, J.C. Patterson, On the response of a reservoir sidearm to diurnal heating and cooling, Journal of Fluid Mechanics 246 (1993) 143–161.
[14] D.E. Farrow, Periodically forced natural convection over slowly varying topography, Journal of Fluid Mechanics 508 (2004) 1–21.
[15] T.P. Bednarz, C. Lei, J.C. Patterson, An experimental study of unsteady natural convection in a reservoir model subject to periodic thermal forcing using combined PIV and PIT techniques, Experiments in Fluids, in press, doi:10.1007/s00348-009-0641-6.
[16] J.D. Hellmus, S.W. Churchill, Simplification of the mathematical description of boundary and initial value problem, AIChE Journal 10 (1964) 110–114.
[17] S.V. Patankar, Numerical Heat Transfer and Fluid Flow, Hemisphere, 1980, ISBN 0-891-16522-3.
[18] H.K. Versteeg, W. Malalasekera, An Introduction to Computational Fluid Dynamics: the Finite Volume Method, Addison Wesley Longman, 1995, ISBN 0-582-21884-5.
[19] B. Van Leer, Towards the ultimate conservative difference scheme. V. A second-order sequel to Godunov's method, Journal of Computational Physics 32 (1979) 101–136.
[20] T.P. Bednarz, C. Lei, J.C. Patterson, Unsteady natural convection in a reservoir model subject to periodic heating and cooling at the water surface, in: XXII International Congress of Theoretical and Applied Mechanics, Adelaide, 2008.
[21] T.P. Bednarz, C. Lei, J.C. Patterson, A numerical study of natural convection induced by iso-flux surface cooling in a reservoir model, International Journal of Heat and Mass Transfer 52 (2009) 56–66.
[22] T. Poinsot, S.M. Candel, The influence of differencing and CFL number on implicit time-dependant non-linear calculations, Journal of Computational Physics 62 (2) (1986) 282–296.